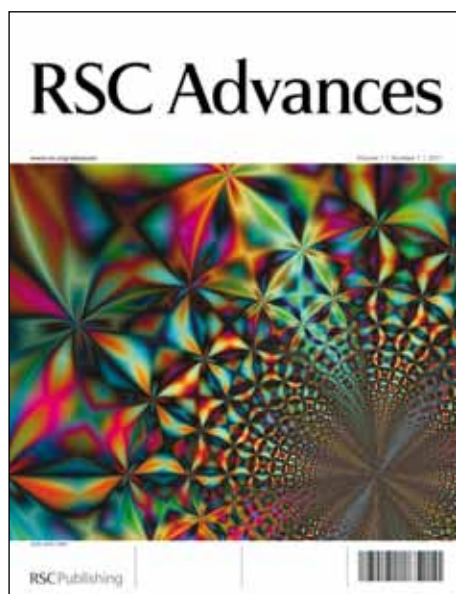


RSC Advances

Accepted Manuscript

This article can be cited before page numbers have been issued, to do this please use: Y. Wen, N. K. Geitner, R. Chen, F. Ding, P. Chen, R. E. Andorfer, P. N. Govindan and P. C. Ke, *RSC Adv.*, 2013, DOI: 10.1039/C3RA43281E.



This is an *Accepted Manuscript*, which has been through the RSC Publishing peer review process and has been accepted for publication.

Accepted Manuscripts are published online shortly after acceptance, which is prior to technical editing, formatting and proof reading. This free service from RSC Publishing allows authors to make their results available to the community, in citable form, before publication of the edited article. This *Accepted Manuscript* will be replaced by the edited and formatted *Advance Article* as soon as this is available.

To cite this manuscript please use its permanent Digital Object Identifier (DOI®), which is identical for all formats of publication.

More information about *Accepted Manuscripts* can be found in the [Information for Authors](#).

Please note that technical editing may introduce minor changes to the text and/or graphics contained in the manuscript submitted by the author(s) which may alter content, and that the standard [Terms & Conditions](#) and the [ethical guidelines](#) that apply to the journal are still applicable. In no event shall the RSC be held responsible for any errors or omissions in these *Accepted Manuscript* manuscripts or any consequences arising from the use of any information contained in them.

Cite this: DOI: 10.1039/c0xx00000x

www.rsc.org/xxxxxx

Communication

Binding of Cytoskeletal Proteins with Silver Nanoparticles

Yimei Wen,^a Nicholas K. Geitner,^a Ran Chen,^a Feng Ding,^b Pengyu Chen,^c Rachel E. Andorfer,^a Praveen Nedumpully Govindan^b and Pu Chun Ke^{*a}

Received (in XXX, XXX) Xth XXXXXXXXXX 20XX, Accepted Xth XXXXXXXXXX 20XX

DOI: 10.1039/b000000x

We have characterized the binding of cytoskeletal proteins, namely, tubulin and actin, with silver nanoparticles using the techniques of dynamic light scattering, UV-Vis spectrophotometry, circular dichroism spectroscopy, hyperspectral imaging, and transmission electron microscopy. Overall, actin displayed a higher propensity than tubulin for silver nanoparticles while both proteins experienced conformational changes upon the binding. Conversely, ion release from silver nanoparticles was significantly compromised upon the formation of protein biocoronas, as shown by inductively coupled plasma mass spectroscopy. The implications of cytoskeletal protein biocorona on the transformation and cytotoxicity of silver nanoparticles have been discussed.

1. Introduction

Recently, it has been established that nanoparticles (NPs), when introduced to a biological environment, readily bind with proteins and natural amphiphiles to render a NP-protein “corona”.^{1,2} The formation of such NP-protein corona, or NP-biocorona in general to encompass the broad interactions between NPs and both biological and environmental species,^{3,4} has been shown to be dynamic (i.e., soft vs. hard corona)⁵⁻⁸ in nature. The origin of the biocorona resides in the physicochemical properties (size, charge, surface coating, and hydrophobicity) of the NPs convolved with the physical (electrostatic, van der Waals, hydrogen-bonding, and hydrophobic) interactions between the NPs and the molecular species constituting the biocorona.^{9,10} A number of recent studies have revealed that the entirety of the NP-biocorona may dictate recognition and uptake of the NPs by membrane receptors and other cellular machineries.¹¹⁻¹³ The association of NPs and proteins may also induce protein aggregation and nucleation that are central to the origins of Alzheimer’s, Creutzfeldt-Jacob disease, and dialysis-related amyloidosis.¹⁴⁻¹⁹ Furthermore, biocorona has been found to mitigate the cytotoxicity of alveolar basal epithelial cells induced by graphene oxide²⁰ and has shown promises for bioimaging and sensing. The implications of NP-biocorona, therefore, encompass the fields of nanoscale assembly, physical chemistry, biophysics, as well as nanotoxicology, bioengineering, and medicine.

It is noted that research on NP-protein corona to date has been primarily focused on plasma proteins^{11,21} and little has been

known regarding the surface modifications of NPs post cell uptake that has broad implications for understanding the fate, transformation, and discharge of NPs. Here we show how major cytoskeletal proteins, tubulin and actin in particular, impact the solubility as well as ion release of silver NPs (AgNPs) through their mutual binding. Actin and tubulin are present in intracellular space in both monomer and polymer form and undergo dynamic exchange, with the vast majority of the proteins present as monomers.²²⁻²⁴ AgNPs are one of the most produced nanomaterials commercially available, owing to their antibacterial and antifungal functions as well as their capability in generating surface plasmon resonance (SPR) for enhanced optical detection and sensing.²⁵⁻²⁷ The cytotoxicity of AgNPs, on the other hand, has been attributed partially to their physical adsorption onto cell membranes/walls and partially to the release of silver ions in the intracellular space which subsequently triggers the production of reactive oxygen species (ROS).²⁸⁻³⁰ In addition, silver ions can also be reduced to AgNPs by physicochemical processes such as cellular metabolism as well as enzymatic activities.^{11,31,32} It is therefore necessary to examine the interactions of cytoskeletal proteins with AgNPs for elucidating the transformation of NPs by ligands in the intracellular environment. In this study, specifically, a collection of physical chemical and analytical techniques, including dynamic light scattering, zeta potential, UV-Vis spectrophotometry, circular dichroism (CD) spectroscopy, hyperspectral imaging, transmission electron microscopy (TEM), and inductively coupled plasma mass spectroscopy (ICP-MS) have been utilized to illustrate the various aspects of the binding of cytoskeletal proteins with AgNPs. We here examine 30 nm, citrate-coated AgNP as they are among the most common types of AgNPs produced. This study expands the scope of our discussion on NP-protein corona from the bloodstream to the intracellular space, and facilitates our understanding of NP-biomolecular interactions and their implications on cell function and cytotoxicity.

2. Experimental

Materials. Citrate-coated AgNPs (Biopure, 30 nm in diameter, 1 mg/mL; equivalent to 11.1 nM per particle) were purchased from NanoComposix (San Diego, CA) and stored at 4°C. Cardiac actin (bovine heart muscle, M.W.: 43 kDa) and tubulin (bovine brain, M.W.: 110 kDa) were purchased from Cytoskeleton (Denver, CO).

The actin was reconstituted to 46.5 μM (2 mg/mL) with distilled water to form a stock solution in the buffer of 5 mM Tris-HCl, pH 8.0, 0.2 mM CaCl_2 , supplemented with 0.2 mM ATP, 5% (w/v) sucrose and 1% (w/v) dextran. The tubulin was dissolved to 10 μM (1.1 mg/mL) by adding 227 μL GTB (General Tubulin Buffer: 80 mM PIPES, pH 6.9, 2 mM MgCl_2 , and 0.5 mM EGTA). The stock actin and tubulin solutions were both stored at -20°C . The structure with electrostatic potentials of both proteins can be found in the Supplementary Information, Fig. S1.

Hydrodynamic size and zeta potential. The hydrodynamic sizes and surface charges of the actin (200 nM), tubulin (50 nM), AgNPs (0.5 nM), actin-AgNPs (400:1 molar ratio), and tubulin-AgNPs (400:1 molar ratio) were determined in standard 1-cm polypropylene cuvettes at room temperature by dynamic light scattering (DLS) (Zetasizer Nano ZS, Malvern Instruments). The cytoskeletal proteins were diluted from the stock solutions by adding deionized water to minimize the influence of salts. The protein-AgNP mixtures were incubated for 2 h at 4°C prior to the measurements.

UV-Vis spectrophotometry. To compare the binding affinity of actin and tubulin for AgNPs, the absorbance spectra of the two types of protein coronas were measured using a UV-Vis spectrometer (Cary 300 Bio, Varian) at room temperature from 350 to 500 nm. Deionized water (18 $\text{M}\Omega\text{-cm}$) was used to dilute stock proteins and AgNPs to produce actin/AgNP mixtures at molar ratios of 50-1500 and tubulin/AgNP mixtures at molar ratios of 20-1500 (AgNPs all 0.1 nM). The cytoskeletal protein-AgNP solutions were incubated for 2 h at 4°C before centrifugation at $8,669 \times g$ for 10 min. The absorbance spectra of the supernatants were then measured using 1-cm path length quartz cuvettes and compared with the SPR spectrum of the AgNPs. The observed spectral red-shifts were attributed to the formation of biocorona (which resulted in an increased local dielectric constant) as well as NP aggregation.

Transmission electron microscopy (TEM) imaging. Direct observation of cytoskeletal protein-AgNPs protein corona was performed on a Hitachi H7600 Transmission electron microscope, operated at a voltage of 120 KV. Specifically, AgNPs (0.1 nM) were incubated with cytoskeletal proteins (40 nM) for 2 h at 4°C before being drop-cast onto a copper grid and dried overnight at room temperature. The proteins were negatively stained for 10 min using phosphotungstic acid prior to imaging. All samples were prepared by directly diluting stock solutions with deionized water.

Hyperspectral imaging. Actin (40 nM) and tubulin (40 nM) each with AgNPs (0.1 nM) were prepared by diluting stock solutions with deionized water and incubated for 2 and 48 h. Hyperspectral images of the samples were collected using an enhanced dark field transmission optical microscope (Olympus BX41) equipped with a hyperspectral imaging spectrophotometer (400-1,000 nm; resolution: 2.8 nm; CytoViva, Auburn, AL). Samples of 10 μL each were wet-mounted on glass slides, covered with #1 coverslips, and completely sealed with lacquer to prevent water evaporation. A hyperspectral image of 0.1 nM AgNPs in the absence of protein was collected as a control. The

spectra for every particle or aggregate in the image were obtained and the peak scattering wavelengths for each particle identified by an automated process. A bin width of 5 nm was used to generate histograms of the peak scattering wavelengths of the samples ranged primarily between 500 to 660 nm. Peak scattering wavelengths less than 500 nm were allocated in the first "500 nm" bin while those larger than 660 nm were grouped in the last "660 nm" bin. The cross correlation between any pair of hyperspectral profiles was computed as the Pearson product-moment correlation coefficient

$$r = \frac{\sum_i (x_i - \bar{x})(y_i - \bar{y})}{\sqrt{\sum_i (x_i - \bar{x})^2} \sqrt{\sum_i (y_i - \bar{y})^2}}, \quad (1)$$

where x_i and y_i correspond to the histogram counts of a given wavelength bin. A correlation coefficient of 1 suggests a high similarity between two spectral measurements, while a correlation coefficient close to 0 denotes low to no similarity.

Circular dichroism (CD) spectroscopy. To probe changes in the secondary structures of actin and tubulin resulting from their binding with the citrate-coated AgNPs, CD measurements were performed at room temperature using a Jasco J-810 spectropolarimeter (Easton, MD). The CD spectra were collected from 190 nm to 300 nm. The protein structures were measured for cytoskeletal proteins (0.25 mg/mL, or 5.8 μM for actin and 2.27 μM for tubulin) and cytoskeletal proteins (0.25 mg/mL) mixed with AgNPs (0.05 mg/mL, 0.555 nM) in deionized water in quartz cuvettes (Starna Cells, Atascadero, CA). To minimize the influence of buffer salts on the measurements, the proteins and protein-AgNP mixtures were directly diluted by deionized water from the stock actin, tubulin, and citrate-coated AgNP suspensions. The protein CD spectra were measured within 1 h of sample preparation to avoid protein denaturation in the absence of salts. The CD spectra of proteins-AgNP were measured after 30 min of incubation. The spectrum of each sample was averaged over three scans taken at 20 nm/min and subtracted by the blanks of deionized water. The measured ellipticity value (θ , in mdeg) was converted to standard units of $\text{deg}\cdot\text{cm}^2/\text{dmol}$ designated as $[\theta]$ using equation $[\theta] = (\theta \cdot M_0) / (10000 \cdot C_{\text{soln}} \cdot L)$, where M_0 is the mean residue molecular weight (114 g/mol), C_{soln} is the protein concentration (g/mL), and L is the path length through the buffer (cm).³³ Once the CD spectra were acquired, they were converted to respective molar ellipticity units to predict secondary structures by the CONTIN/LL and CDSSTR methods afforded by the CDPro package, using the SP43 and SP48 protein reference datasets. Each of the deconvoluted spectra were then assessed for quality by analyzing the R-fit using non-linear regression. The final secondary structures represented the averaged structures obtained from all of the reliable outputs (R-fit < 10) resulting from the data analysis.

Inductively coupled plasma mass spectrometry (ICP-MS). AgNPs in aqueous readily release silver ions over time, and the rate of this dissolution may be greatly reduced by capping agents or a biocorona on the particle surface. Direct observation of the release rate of silver ions by AgNPs was performed using ICP-MS (X Series 2, Thermo Scientific). Specifically, AgNPs (5 mg/L, 0.0555 nM) were incubated with actin (5 mg/L, 116 nM) or

tubulin (5 mg/L, 45 nM) after directly diluting the stock solutions with deionized water. After incubating for up to 72 h, the cytoskeletal protein-AgNPs mixtures were centrifuged twice at 12,100 \times g for 30 min and their supernatants were collected. The supernatants were then diluted with 2% HNO₃ and measured in triplicate by ICP-MS using a standard silver ion solution and ⁴⁵Sc and ⁶⁹Ga as internal standards.

3. Results and discussion

As shown in Table 1, the zeta potentials of proteins-AgNPs are closer to that of proteins than to AgNPs. This is due to the coating of cytoskeletal proteins on the AgNPs as well as free proteins, as reflected by the TEM images (Fig. 2). Actin and tubulin both yielded high standard deviations for their zeta potentials (Table 1), possibly due to self-aggregation and minor polymerization. In addition, actin-AgNP displayed a smaller standard deviation in zeta potential than tubulin-AgNP (Table 1), implying that the actin-AgNP biocorona was more homogeneous than the tubulin-AgNPs biocorona.

Table 1. Hydrodynamic sizes and zeta potentials of AgNPs and cytoskeletal protein-AgNPs.

	Hydrodynamic size (nm)	Zeta potential (mV)
AgNPs	35.7 \pm 0.2	-42.5 \pm 0.1
Actin	-2.0	-28.0 \pm 5.6
Actin-AgNPs	39.4 \pm 0.7	-31.6 \pm 0.8
Tubulin	-9.0 (aggregation)	-27.1 \pm 3.3
Tubulin-AgNPs	44.8 \pm 0.6	-27.0 \pm 2.6

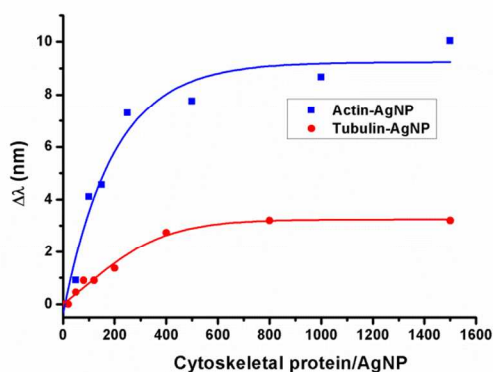


Fig. 1 Red-shifts of UV-Vis absorbance peak wavelengths induced by the formation of cytoskeletal protein-AgNP biocorona, in reference to that for AgNPs alone at $\lambda_0 = 406$ nm. The horizontal axis shows the molar ratios of cytoskeletal proteins to AgNPs.

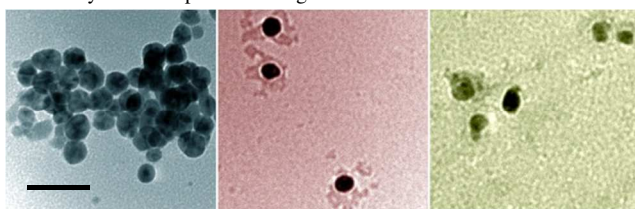


Fig. 2 TEM imaging of (left) citrate-coated AgNPs, (middle) actin-AgNP, and (right) tubulin-AgNP biocorona. Scale bar: 100 nm.

Actin (polydispersity index or PDI: 0.659) and tubulin (PDI: 0.662) displayed broad size distributions in their buffers. However, the proteins-AgNPs were more uniform in size (PDI: 0.286 for actin-AgNP and 0.290 for tubulin-AgNP), evidently due to the breakage of protein aggregates by the AgNPs. The hydrodynamic size of actin-AgNPs increased by 3.7 nm than AgNPs (~twice the hydrodynamic size of actin), indicating coating of a single actin layer on the AgNPs. In comparison, the hydrodynamic size of tubulin-AgNP increased by 9.1 nm (~the hydrodynamic size of tubulin) than AgNPs, suggesting that the AgNPs were partially coated by a single layer of tubulin. These results agree qualitatively with the UV-Vis absorbance and TEM data (Figs. 1 and 2). By comparing the UV protein absorbance intensities (280 nm for tubulin, 260 nm for actin) after 2h incubation of proteins with AgNPs (1500:1 molar ratio) and removing all AgNPs and strongly bound cytoskeletal proteins by centrifugation and comparing to control protein UV-Vis spectra, we concluded that AgNPs have a strong binding capacity for 150 and 300 tubulin and actin molecules per particle, respectively. This further suggests that monolayers being formed on the nanoparticle surfaces. The smaller size and greater flexibility of actin (~2 nm) compared to tubulin (~9 nm) as well as the hydrodynamic size data suggest that actin results in more complete surface coverage of the AgNPs. This explains the greater SPR redshift seen in Fig. 1, as a larger degree of surface coverage by proteins will result in a more significant change in the local dielectric constant, resulting in a more significant redshift of the AgNP SPR.

Hyperspectral imaging combines high signal-to-noise dark field microscopy with high-resolution scattering spectra for each pixel (Supporting Information, Fig. S2) and has been employed recently for the detection of NPs and their aggregations.³⁴⁻³⁶ Since protein coating induced red-shifts in the SPR spectra of the AgNPs, red-shifts also occurred in the peak scattering wavelengths for protein-coated AgNPs than AgNPs alone. Our hyperspectral imaging showed a maximum spectral peak at 550 nm for the AgNPs (Fig. 3, orange bars in top and middle panels), as a result of AgNP self aggregation. In comparison, a slight blue-shift was observed for actin-AgNPs with 2 h incubation and a further enhanced blue-shift was observed for actin-AgNP with 48 h incubation, likely through continued breakage of AgNP aggregates over time (Fig. 3, top and lower panels). Indeed, the cross-correlations of the hyperspectral histograms for actin-AgNP at 2 h and 48 h with AgNPs at 2 h are 0.97 and 0.24, respectively. In contrast, the spectra of tubulin-AgNP after 2 h incubation yielded a broader distribution compared with AgNPs alone (Fig. 3 middle panel, orange vs. green bars), likely caused by self-aggregation and polymerization of the tubulin. Like actin, tubulin also facilitated the breakdown of AgNP aggregates, though less effectively (Fig. 3, middle vs. top panel, see counts for wavelengths below 550 nm) and displaying no apparent time dependence (cross correlations with AgNPs at 0.63 vs. 0.60, Fig. 3 lower panel), which indicates that the biocorona were stable in solution and did not dissociate or degrade with time.

The secondary structures of actin and tubulin were altered resulting from their interactions with the AgNPs (Fig. 4, Fig. S3,

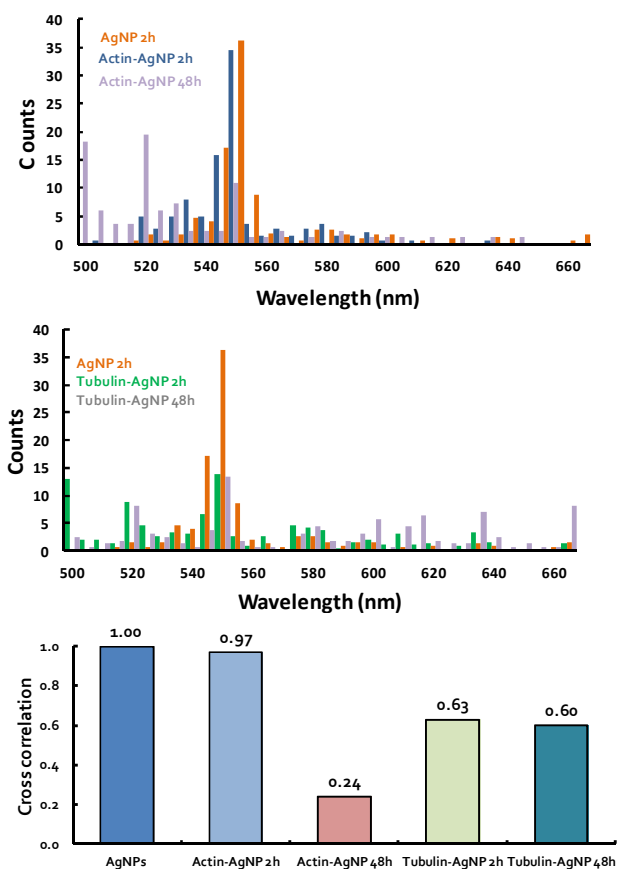


Fig. 3 (Top and middle panels) Histograms of the hyperspectra of AgNPs and cytoskeletal protein-AgNPs. Bin width: 5 nm. A total number of 82 to 359 NPs or NP with protein aggregates were screened in each case to derive the histograms. (Bottom panel) Cross correlations of the hyperspectra of cytoskeletal protein-AgNPs with that of AgNPs.

Table S1). Specifically, the alpha helices of actin showed a 24% relative decrease (from 38% to 29%) while beta sheets a 36% relative increase (from 25% to 34%) upon their binding to the AgNPs. No changes were observed for the percent of random coils. In comparison, the alpha helices of tubulin displayed a 17% relative decrease (from 35% to 29%), beta sheets a 5% relative increase (from 21% to 22%), and random coils an 11% increase once bound to the AgNPs. In other words, both actin and tubulin showed a decrease in alpha helices and an increase in beta sheets upon biocorona formation, similar to that observed for tubulin exposed to hydroxylated fullerene.³⁷ In addition, the conformational changes were greater for actin than tubulin, consistent with our UV-Vis absorbance measurement and hyperspectral imaging (Figs. 1 and 3).

The differential binding of actin and tubulin for AgNPs, as reflected by the absorbance, hyperspectral imaging, and CD measurements, can be derived from the discrepancies in the physicochemical and structural properties of the two types of cytoskeletal proteins. Since both actin and tubulin are rich in alpha helices (both at 35%) and turns and their zeta potentials were nearly identical, at approximately -27 to -28 mV (Table 1), we attribute the observed differential binding to the differences in the rigidity and size of the two types of proteins. Structurally, actin is a globular protein of 43 kDa while tubulin is an alpha-

beta dimer of 110 kDa. Both actin and tubulin can be polymerized into microfilaments and microtubules respectively under favourable conditions, with microtubules possessing a higher rigidity and a much longer persistence length than actin filaments.³⁸ In the cell, actin carries out more interactions than most other proteins and it is conceivable that actin bound more efficiently to citrate-coated AgNPs than tubulin. Such binding is likely realized via hydrogen bonding between the citrate coating of the AgNPs and the abundant peripheral alpha helices and turns of the proteins, in addition to electrostatic, van der Waals, and hydrophobic interactions between the two species, similar to what we observed for AgNP-ubiquitin biocorona.³⁹ The hydrogen bonding with citrate-coated AgNPs perturbed the structural integrity of the alpha helices and turns that populated the protein surfaces, as reflected by our CD measurements for both actin and tubulin (Fig. 4). Due to the highly localized nature of hydrogen bonding (typically 2-3 angstroms in bond length), the larger sized tubulin should be less efficient than actin for their binding to the AgNPs that possessed a significant curvature. The effect of NP size on binding energies and conformational changes in cytoskeletal proteins is a subject of future discrete molecular dynamics (DMD) studies; it is expected that smaller NPs will cause more conformational changes compared to larger particles and will favour binding by smaller, more flexible proteins.¹⁴ Furthermore, as a non-covalent capping agent, citrate could undergo rapid and stochastic exchanges with the cytoskeletal proteins in aqueous for adsorbing onto the AgNPs. Sterically, the smaller actin should be more flexible than tubulin in occupying the AgNP surface areas transiently free from citrate coating, through electrostatic and hydrophobic interactions. Previous experimental⁴⁰ and our computational³⁹ studies have shown that AgNPs prefer to bind to negatively charged protein surfaces. Such potential binding sites are highlighted as clusters on tubulin and actin, with their residues specified in Fig. S1.

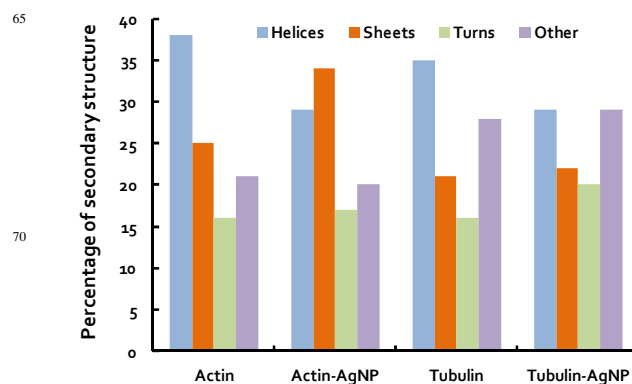


Fig. 4 Changes in the secondary structures of actin and tubulin upon their binding with AgNPs. Note the consistent decreases in alpha helices and increases in the beta sheets for both types of proteins when bound to the AgNPs.

As shown in Fig. 5, without the presence of cytoskeletal proteins (black curve) AgNPs rapidly released silver ions, from 0.13 to 0.20 mg/L within the first 4 h, while the rate of release levelled off subsequently for the total observation period of 72 h. The released silver ions reached a concentration of ~0.27 mg/L at 72 h for an original AgNP concentration of 5 mg/L, implying a

~5% dissolution of the NPs. In the presence of actin and tubulin (blue and red curves), in contrast, the release of silver ions progressed at a slower pace, from ~0.06 to 0.08 mg/L during the first few hours. Such ion release was then briefly saturated, reduced, and levelled off to a final concentration of ~0.05 mg/L, or ~20% of that released by AgNPs over 72 h without the presence of proteins. This measurement implies that the coating

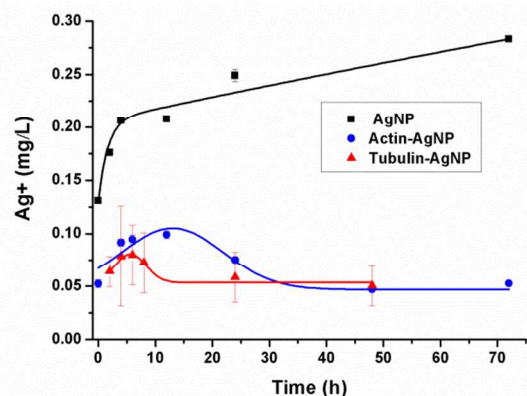


Fig. 5 Release of silver ions with and without the presence of proteins, measured (n=3) by ICP-MS. Original AgNP concentration: 5 mg/L. Actin and tubulin concentrations: 5 mg/L.

of cytoskeletal proteins on the AgNPs physically hindered the release of silver ions, and the dynamic process of biocorona formation competed with and eventually dominated silver ion release to stabilize the AgNPs. This time-dependent result further suggests that the conformation and physicochemical properties of AgNPs are better preserved by hardened cytoskeletal proteins. However, it also implies that the formation of this biocorona alone is insufficient to fully scavenge silver ions that are a major cause of triggering ROS production and cytotoxicity.

4. Conclusions

In summary, we have shown that cytoskeletal proteins can interact readily with citrate-coated 30 nm AgNPs, likely through hydrogen bonding, electrostatic, van der Waals, and hydrophobic interactions. Changes in the size and surface coating are expected to affect protein binding energies¹⁴ and electrostatic interactions and are the subject of ongoing study. In general, actin showed a higher propensity than tubulin for binding with the 30 nm citrated-coated AgNPs, likely originated from their smaller size and less rigidity. Binding with AgNPs induced changes in the secondary structures for both types of proteins, while compromised silver ion release from the AgNPs as a result of biocorona formation and hardening. The knowledge derived from this study may facilitate our understanding of the fate and transformation of nanomaterials in mammalian and plant cells,⁴¹ and should have relevance to the field studies of NP-biomolecular interaction, toxicology, biosensing, and medicine involving metallic NPs.

Acknowledgments

This research was supported by NSF grant #CBET-1232724 to

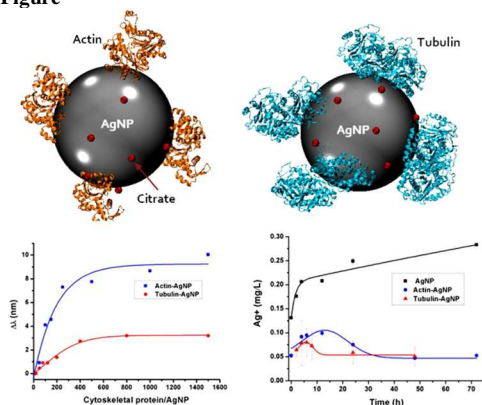
Ke, an NSF-REU grant to Andorfer, and Clemson University startup funds to Ding. The authors thank Aby Thyparambil and Rhonda Powell for assisting the CD and hyperspectral imaging measurements.

Notes and references

- ^aNano-Biophysics and Soft Matter Laboratory, Clemson University, Clemson, SC, 29634, USA. Fax: 1-864-6560805; Tel: 1-864-656-0558; E-mail: puchunkesp@gmail.com.
- ^bStructure, Dynamics, and Function of Biomolecules and Molecular Complexes Laboratory, Clemson University, Clemson, SC, 29634, USA.
- ^cMicrosystems Technology and Science Laboratory, University of Michigan Ann Arbor, MI, 28109, USA.
1. T. Cedervall, I. Lynch, S. Lindman, T. Berggard, E. Thulin, H. Nilsson, K. A. Dawson, and S. Linse, *Proc. Natl. Acad. Sci. USA*, 2007, **104**, 2050.
 2. I. Lynch, A. Salvati, and K. A. Dawson, *Nature Nanotech.*, 2009, **4**, 546.
 3. Food and Agricultural Organization of the United Nations, World Health Organization. *FAO/WHO Meeting Report* (Rome), 2010, 38.
 4. S. Radic, N. K. Geitner, R. Podila, A. Kallinen, P. Chen, P. C. Ke, and F. Ding, *Scientific Reports*, 2013, **3**, 2273.
 5. M. Lundqvist, J. Stigler, T. Cedervall, T. Berggard, M. B. Flanagan, I. Lynch, G. Elia, and K. Dawson, *ACS Nano*, 2011, **5**, 7503.
 6. E. Casals, T. Pfaller, A. Duschl, G. J. Oostingh, and V. F. Puentes, *Small*, 2011, **7**, 3479.
 7. F. D. Sahneh, C. Scoglio, and J. Riviere, *PLoS ONE*, 2013, **8**, e64690.
 8. S. Milani, F. B. Bombelli, A. S. Pitek, K. A. Dawson, and J. Radler, *ACS Nano*, 2012, **6**, 2532.
 9. X. R. Xia, N. A. Monteiro-Riviere, S. Mathur, X. Song, L. Xiao, S. J. Oldenberg, B. Fadeel, and J. E. Riviere, *ACS Nano*, 2011, **5**, 8449.
 10. A. E. Nel, L. Mädler, D. Velegol, T. Xia, E. M. Hoek, P. Somasundaran, F. Klaessig, V. Castranova, and M. Thompson, *Nature Mater.*, 2009, **8**, 543.
 11. M. P. Monopoli, C. Åberg, A. Salvati, and K. A. Dawson, *Nature Nanotech.*, 2012, **7**, 779.
 12. A. Lesniak, F. Fenaroli, M. P. Monopoli, C. Åberg, K. A. Dawson, and A. Salvati, *ACS Nano*, 2012, **6**, 5845.
 13. R. Gaspar, *Nature Nanotech.*, 2013, **8**, 79.
 14. L. Fei and S. Perrett, *Inter. J. Mol. Sci.*, 2009, **10**, 646.
 15. S. Auer, A. Trovato, and M. Vendruscolo, *PLoS Comput. Biol.*, 2009, **5**, e1000458.
 16. E. P. O'Brien, J. E. Straub, B. R. Brooks, and D. Thirumalai, *J. Phys. Chem. Lett.*, 2011, **2**, 1171.
 17. Z. J. Deng, M. Liang, M. Monteiro, I. Toth and R. F. Minchin, *Nature Nanotech.*, 2011, **6**, 39.
 18. N. Gao, Q. Zhang, Q. Mu, Y. Bai, L. Li, H. Zhou, E. R. Butch, T. B. Powell, S. E. Snyder, G. Jiang, and B. Yan, *ACS Nano*, 2011, **5**, 4581.
 19. A. Salvati, A. S. Pitek, M. P. Monopoli, K. Prapainop, F. B. Bombelli, D. R. Hristov, P. M. Kelly, C. Åberg, E. Mahon, and K. A. Dawson, *Nature Nanotech.*, 2013, **8**, 137.
 20. W. Hu, C. Peng, M. Lv, X. Li, Y. Zhang, N. Chen, C. Fan, and Q. Huang, *ACS Nano*, 2011, **5**, 3693.
 21. S. Yang, Y. Liu, Y. Wang, and A. Cao, *Small*, 2013, **9**, 1635.
 22. C. E. Walczak, *Curr. Opin. Cell Biol.*, 2000, **12**, 52.
 23. T. Kiushi, T. Nagai, K. Ohashi, and K. Mizuno, *J. Cell Biol.*, 2011, **193**, 365.
 24. T. D. Pollard, L. Blanchion, and R. D. Mullins. *Biophysics and Biomolecular Structure*. **29**, 545.
 25. X. Jin, M. Li, J. Wang, C. Marambio-Jones, F. Peng, X. Huang, R. Damoiseaux, and E. M. V. Hoek *Environ. Sci. Technol.*, 2010, **44**, 7321.
 26. O. Choi and Z. Hu, *Environ. Sci. Technol.*, 2008, **42**, 4583.
 27. A. Kennedy, M. Hull, A. J. Bednar, J. Goss, J. Gunter, J. Bouldin, P. Vikesland, and J. Steevens, *Environ. Sci. Technol.* 2010, **44**, 9571.
 28. W. Zhang, Y. Yao, N. Sullivan, and Y. Chen, *Environ. Sci. Technol.* 2011, **45**, 4422.

29. G. A. Sotiriou and S. E. Pratsinis, *Environ. Sci. Technol.* 2010, **44**, 5649.
30. S. Kittler, C. Greulich, J. Diendorf, M. Koller, and M. Epple, *Chem. Mater.*, 2010, **22**, 4548.
31. N. Duran, P. D. Marcato, O. L. Alves, G. I. H. De Souza, and E. Esposito, *J. Nanobiotechnology*, 2005, **3**, 8.
32. K. Juganson, M. Mortimer, A. Ivask, K. Kasemets, and A. Kahru, *Environ. Sci.: Processes Impacts*, 2013, **15**, 244.
33. N. Sreerama and R. W. Woody, *Anal. Biochem.*, 2000, **287**, 252.
34. A. R. Badireddy, M. R. Wiesner, and J. Liu, *Environ. Sci. Technol.*, 2012, **46**, 10081.
35. M. Hu, C. Nova, A. Funston, H. Wang, H. Staleva, S. Zou, P. Mulvaney, Y. Xia, and G. V. Hartland, *J. Mater. Chem.*, 2008, **18**, 1949.
36. K. Seekell, M. J. Crow, S. Marinakos, J. Ostrander, A. Chilkoti, and A. Wax, *J. Biomed. Opt.* 2011, **16**, 116003.
37. T. A. Ratnikova, P. N. Govindan, E. Salonen, and P. C. Ke, *ACS Nano*, 2011, **5**, 6306.
38. F. Gittes, B. Mickey, J. Nettleton, and J. Howard, *J. Cell Biol.*, 1993, **120**, 923.
39. F. Ding, S. Radic, R. Chen, P. Chen, N. K. Geitner, J. M. Brown, and P. C. Ke, *Nanoscale*, 2013 (DOI: 10.1039/c3nr02147e).
40. L. Calzolari, F. Franchini, D. Gilliland, and F. Rossi, *Nano Lett.*, 2010, **10**, 3101.
41. P. C. Ke and M. H. Lamm, *Phys. Chem. Chem. Phys.*, 2011, **13**, 7273.

TOC Figure



(Top row) Illustrations of actin and tubulin bound with a silver nanoparticle (AgNP) (not in proportion). Also shown are citrates (red) adsorbed onto the NP surface. (Lower row, left to right) SPR spectral shifts of AgNPs and hindered silver ion release as a result of protein coating and hardening.